Torsional capacity of ultra-high-performance concrete beams using rectangle stirrup

Xia Cao [a], Wei-Jia Zhang [a], Yi-Cheng Ren [a,b], Feng Fu [c,*], Yu-hua Li [a,**], Da-Bo He [d], Yan Zheng [a]

[a] *Guang Xi Key Laboratory of New Energy and Building Energy Saving, Guilin University of Technology, Guilin, 541004, China*
[b] *Construction Institute, Guangdong Technology College, Zhaoqing, 526000, China*
[c] *Department of Engineering, School of Science and Technology , City University of London, EC1V 0HB, UK*
[d] *Construction Institute, Nanning College Of Technology, Guilin, 541004, China*

A R T I C L E   I N F O

Keywords:
Ultra-high-performance concrete beam
Rectangle stirrup
Torsional performance
Torsion reduction coefficient

A B S T R A C T

This study studies the torsional capacity of rectangular ultra-high-performance-concrete (UHPC) beams. Nine UHPC beams were tested under pure torsion load. The failure modes were presented and the influences of parameters, including reinforcement ratio, stirrup ratio and steel fiber content were discussed. The experimental results showed that longitudinal reinforcement ratio had little effect on crack width and plastic stiffness in serviceability stage. Increasing the stirrup ratio and steel fiber content effectively inhibited the development of crack width and improved plastic stiffness. The torsional ductility of UHPC beams decreased with the increase of longitudinal reinforcement ratio but increased with the increase of stirrup ratio and steel fiber content. The cracking torque and elastic stiffness of UHPC beams were less affected by the reinforcement ratio and increased with the increase of steel fiber content. The twist, energy consumption, and ultimate torque of UHPC beams increased with the increase of longitudinal reinforcement ratio, stirrup ratio, and steel fiber content. The damage index of UHPC beams was 0.85–0.90, and the plastic stiffness accounts for 1/25–1/10 of the elastic stiffness.

1. Introduction

Relevant scholars and experts have done many research on flexural and shear behavior of UHPC members [1–4], while the little attention has been paid to torsional performance. In the past, increasing stirrups and longitudinal reinforcement ratio resisted the torque of the members. With the development and application of new materials, the building components are developing towards light-weight, high-strength and assembly. The building structure becomes more higher, complex and flexible. The torsion problem of the components cannot be ignored.

For torsion in concrete beams, Hong [5] carried out pure torsion test on reinforced concrete (RC) beams and found the torsional failure law of RC beams. Lopes et al. [6] conducted torsion test of high-strength concrete hollow beams. The results showed that the torsional ductility only occured for the narrow interval of torsional reinforcement. Rahal et al. [7] presented a simple non-iterative model for calculating the ultimate torsional strength of ordinary and high-strength concrete members, combining the influence of longitudinal reinforcement, stirrup, concrete compressive strength and cross-sectional area. However, the poor tensile strength and

brittleness of ordinary concrete and high-strength concrete limit application in torsion members. The steel fiber was added to form fiber concrete, increasing the tensile strength of concrete and decreasing the brittleness of concrete. Rao et al. [8] found that adding steel fibers could improve the torsional strength and ductility through the torsional test of steel fiber reinforced concrete beams. Okay et al. [9] analyzed the influence of steel fiber content, fiber length width ratio and longitudinal reinforcement on the torsional performance of steel fiber reinforced concrete beams. The results showed that the energy absorption capacity was significantly affected by the steel fiber. Karimipour et al. [10] found that polypropylene fibers improved torsional behavior comparing to steel fibers for high performance concrete beams. UHPC is a new type of cement-based composite material composed of high-density matrix and steel fiber made according to the maximum bulk density theory [11,12], which has been widely used in bridges, buildings, nuclear power, municipal, marine and other projects [13–15]. UHPC is different from ordinary concrete and high-strength concrete. The "bridging" effect of steel fiber makes UHPC show different characteristics under torque. The high density of the UHPC matrix allows for better tensile action and tensile efficiency of the fibers in the concrete matrix, which makes UHPC different from fiber concrete.

UHPC has also been used in torsional specimens. Yang et al. [16] found that the torsional strength of UHPC beams increased with the increase of steel fiber content, stirrup ratio and longitudinal reinforcement ratio. Alamli et al. [17] tested the torsional performance and load carrying capacity of hollow activated powder concrete T-beams. The results showed that 2% of steel fibers significantly improved the cracking torque and ultimate torque of hollow activated powder concrete T-beams. Ibrahim et al. [18] found that the failure mode was controlled by combination of oblique concrete crushing and spalling of concrete cover when the concrete cover was small, and by spalling of concrete cover when the concrete was concrete cover large. Mohammed et al. [19] found that UHPC jackets could delay the formation of cracks and improved the torsional load capacity of the torsional beam. Zhou et al. [20] concluded that the cracking torque of the test beam depended mainly on the section size and was less influenced by the wall thickness and section type. The flange plate could improve the torsional strength and reduced the torsional deformation according to the flange UHPC hollow beam torsion test. Zhou et al. [21] found the mixing effect of steel fibers. The cracking and ultimate torque of mixed steel fiber UHPC beams were higher than that of single steel fiber beams. Fehling [22] experimentally found that the steel fiber content exceeded 0.9% to achieve an effective load-bearing mechanism after cracking together with the longitudinal reinforcement.

At present, the influence mechanism of longitudinal reinforcements, stirrups and steel fiber content on the torsional performance of UHPC beams is unclear, and various factors affect each other. To evaluate the synergy between the research variables and UHPC from the aspect of torsional performance, the torsional response of UHPC beams in terms of longitudinal reinforcement ratio, stirrup ratio and steel fiber content were investigated in this study, and the nine UHPC beams were fabricated and tested. The stress characteristics of reinforcement and UHPC at different loading times were revealed and the role of steel fiber in the torsion process was explored. The applicability of the current calculation formula for concrete torsion was verified, and the calculation formula for torsional bearing capacity of UHPC beams was proposed.

2. Experimental program

2.1. Material property

The mix proportion of UHPC used in the test is presented in Table 1. The materials included silica sand, cement (PO42.5), silica fume, steel fiber, superplasticizer and water. The material properties are summarized in Table 2.

The preparation process of UHPC beams was as follows: First place the wood mold on the ground and keep the level. Meanwhile, the three grades of silica sand were pre-mixed for 2 min. Before, the steel fibers were added and mixed for another 2 min. Then, cement and silica fume were added and mixed for 10 min. Next, superplasticizer and water were put in and stirred for 6 min. At the end, mixed UHPC was placed from one end of the wooden mold and allowed to flow freely, and the beams were smoothed out and maintained for 28 days.

Meanwhile, specimens were poured to measure the mechanical properties of UHPC. Standard specimens, 100mm × 100mm × 100mm, were continuously and uniformly loaded (rate of 1.2 MPa/s) until destruction, measuring the UHPC cubic compressive strength. The pouring surface of specimens was perpendicular to the loading direction during loading. Standard specimens, 100mm × 100mm × 100mm, were placed in the concrete splitting tensile test fixture. Specimens were continuously and uniformly loaded (rate of 0.12 MPa/s) until the specimen failed, measuring the splitting tensile strength of the UHPC cube. The centerline of the fixture was coincident with the center of the press plate. A prism of 150mm × 150mm × 300mm was used to conduct the UHPC elastic modulus test in response to the GB/T31387-2015 [23], as shown in Fig. 1. The mechanical properties of UHPC are given in Table 3.

The diameter of HRB400 steel bars used in the test beams were 10 mm, 12 mm, 14 mm and 16 mm. The mechanical properties of steel bars are shown in Table 4.

2.2. Specimen preparation

In order to study the effect of longitudinal reinforcement ratio, stirrup ratio and steel fiber content on the torsional performance of

Table 1
Mix design of UHPC.

Materials	Cement	Silica sand			Silica fume	Superplasticizer	Water	Steel fibers
		Coarse sand	Medium sand	Fine sand				
mix proportion	1	0.2	0.8	0.2	0.3	0.02	0.23	0.75%/1.5%/3%

Where:Steel fiber is the volume dose, others are mass dose.

Table 2
Material properties.

Materials	Material properties
Silica sand	Coarse sand (0.63–1.25 mm), Medium sand (0.315–0.63 mm), Fine sand (0.16–0.315 mm)
Cement	Portland cement (PO42.5)
Silica fume	Silica flour with 98% SiO_2 at 0.3 μm average diameter
Steel fibers	Diameter:0.2 mm and length:13 mm, Smooth and straight steel fiber
Superplasticizer	The water reduction rate of polycarboxylate superplasticizer is 29%

(a)

(b)

(c)

Fig. 1. UHPC mechanical properties tests; (a) concrete cube compressive strength, (b) concrete cube splitting tensile strength, (c) UHPC elastic modulus.

Table 3
Mechanical properties of UHPC.

Steel fiber content	f_t(MPa)	f_c(MPa)	E_c(GPa)
0.75%	4.22	116.20	42.5
1.5%	7.10	123.76	44.2
3%	7.91	131.58	45.6

Where: f_t is the tensile strength of UHPC; f_c is the cubic compressive strength of UHPC; E_c is the elastic modulus of UHPC.

Table 4

Mechanical properties of HRB400 reinforcement.

d (mm)	A (mm)	f_y (MPa)	f_u (MPa)
10	78.5	467.1	611.4
12	113.1	452.4	603.4
14	153.9	447.9	598.1
16	201.1	441.7	602.3

Where: d is diameter of rebar, A is area of rebar, f_y is yield strength of rebar, f_u is ultimate strength of rebar.

UHPC beams, nine steel rebars reinforced UHPC beams were designed. The test beams are 2100 mm in length and 1200 mm in pure torsional test section. To prevent the failure of the beams outside the purely torsion zone, the stirrup encrypted zone was set at both ends of beams. The length of the encryption zone was 450 mm, and the spacing of stirrup was 50 mm. The concrete cover was 20 mm. The dimensions and reinforcement are shown in Fig. 2 and Table 5. The UHPC beams were named according to the longitudinal reinforcement ratio, stirrup ratio and steel fiber content. L represented the longitudinal reinforcement ratio, S represented the stirrup ratio, and F represented the steel fiber content. For example, L121S126F075 represented UHPC beams with longitudinal reinforcement ratio of 1.21%, stirrup ratio of 1.26%, and steel fiber content of 0.75%.

2.3. Test set up

The locations of the steel strain gauges are shown in Fig. 3. Strain gauges were placed at the fourth-order point of longitudinal reinforcement in test section to measure the strain of longitudinal reinforcement. Apply strain gauges at the midpoint of the four sides of the stirrups and measure the strain of the stirrups. Rosettes were pasted at the quarter points of the UHPC beam test section to measure the concrete strain. Inclinometers were placed at the start and end points of the UHPC beams test section as well as at the quadrature points to measure the beams rotational angle, as shown in Fig. 4. The accuracy of inclinometer is $0.05°$ (0.00087 rad). The surface of the UHPC beam was whitened and divided into a grid before testing, and the crack observation instrument was used to observe and record the development of cracks during the test.

The experiment was conducted at Guilin University of Technology. Static loading was carried out by hydraulic jack, as depicted in Fig. 5. The steel plates with holes on both sides were placed on the rollers, and the bolts that keeping the steel plates balanced were installed on both sides of the steel plates. After the steel plates on both sides were adjusted to the same horizontal position, the UHPC beam was assembled on the steel plate. Steel cantilever beams were assembled on both sides of the UHPC beam. The cantilever beams and the bottom steel plate were fixed with bolts, so the test beam could rotate with the cantilever beam. The pressure transducer and jack were fixed at the geometric center position on the upper surface of the distribution beam and lifted together to the counterforce frame. The bottom balancing bolt was removed when loading. The 200 KN hydraulic jack was used to apply vertical load to the distribution beam to achieve the torsion of both ends of the test beam at the same time. The length of the torsion arm was 0.61 m in the initial state.

The test was implemented by applying staged loading. The cracking torque of the test beams was estimated. Before reaching 80% of the predicted cracking torque, the loading value of each stage was 10% of the predicted cracking torque. When approaching the cracking torque, each stage was loaded at 5% of the cracking torque, and the load was increased to 10% of the cracking torque at each stage after cracking. To ensure the full development of the crack, the load of each increment was maintained for 5–10 min.

3. Experimental phenomena

The failure modes of the UHPC beams are illustrated in Fig. 6(a). The failure modes of UHPC beams were divided into two types: brittle failure and ductile failure. L00S00F075 and L121S00F075 were not equipped with stirrups, and the failure occurs quickly after
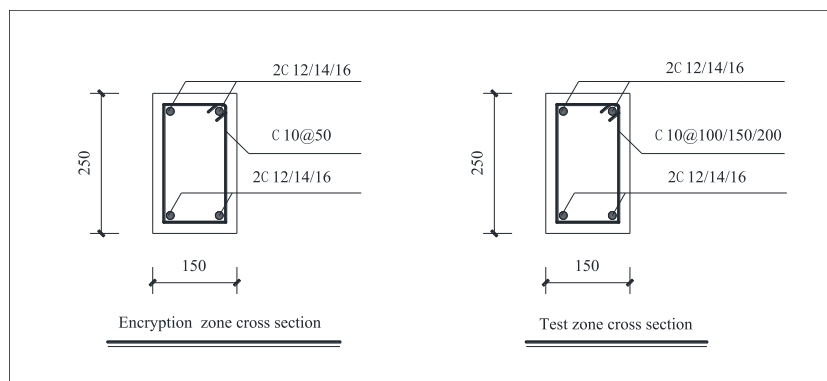

Fig. 2. Section details of test beams.

Table 5

Main parameters of UHPC beams.

Beams	$b \times h$/mm²	L/mm	ρ %	ρ_{sv} %	ζ	ρ_s %
L00S00F075	150 × 250	2100	0	0	–	0.75
L121S00F075	150 × 250	2100	1.21 (4C 12)	0	–	0.75
L121S126F075	150 × 250	2100	1.21 (4C 12)	1.26(C 10@100)	1.03	0.75
L164S126F075	150 × 250	2100	1.64 (4C 14)	1.26(C 10@100)	1.40	0.75
L214S126F075	150 × 250	2100	2.14 (4C 16)	1.26(C 10@100)	1.83	0.75
L121S084F075	150 × 250	2100	1.21 (4C 12)	0.84(C10@150)	1.54	0.75
L121S063F075	150 × 250	2100	1.21 (4C 12)	0.63(C 10@200)	2.06	0.75
L121S084F150	150 × 250	2100	1.21 (4C 12)	0.84(C 10@150)	1.54	1.50
L121S084F300	150 × 250	2100	1.21 (4C 12)	0.84(C 10@150)	1.54	3.00

Where: b is the beam width, h is beam height, L is the beam span, ρ is the longitudinal reinforcement ratio, ρ_{sv} is the stirrup ratio, ζ is the reinforcement strength ratio, ρ_s is the content of steel fiber.
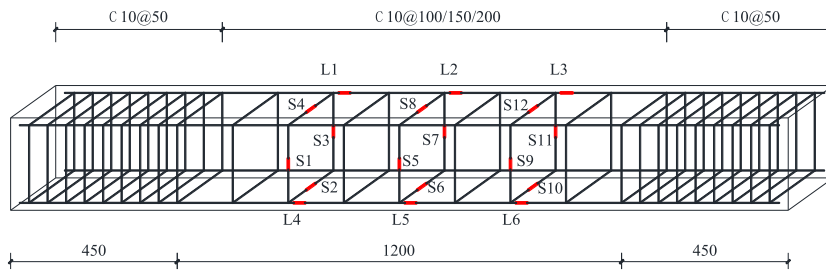
Where: L1-L7 represent the longitudinal reinforcement strain gauges. S1-S12 represent the stirrup strain gauges.

**Fig. 3.** Reinforcement strain gauge arrangement.
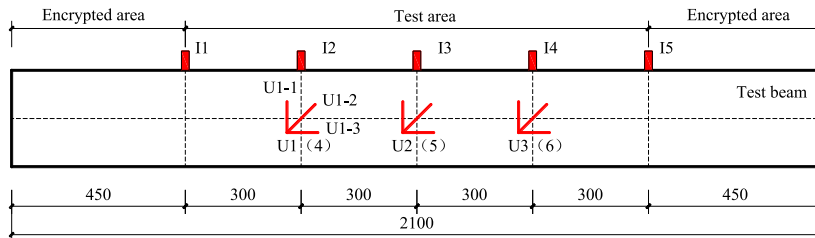
Where: UI, U2, U3 represent the concrete strain gauges on the side of the UHPC beam and U4, U5, U6 on the other side.

Fig. 4. Inclinometer, concrete strain gauge arrangement.

cracking. This type of brittle damage was characterized rapidly and suddenly. However, the configuration of longitudinal reinforcement made the internal force distribution more uniform and the damage range greater when the test beam was damaged, as shown in Fig. 6(b) and (c). After cracking of other test beams, many parallel cracks were slowly added with the increase of load. Finally, the test beams were damaged with the widening of an inclined crack in the pure torsion section. This type of ductile damage was characterized slowly and obvious failure warning. The different amount of reinforcement and steel fiber content resulted in the different number of helical cracks under the action of torque. The UHPC beams with stirrups ratio of 1.26% had denser cracks on the surface of the beams at failure and only had one main crack. However, the cracks on the surface of the test beam were sparser when the UHPC beams with 0.63% and 0.84% stirrups ratio were damaged, and the test beam had two parallel main cracks. This indicates that the restraining power of the concrete in the core area was weakened by the large spacing of stirrups. Compared with L121S084F075, two large cracks of L121S084F150 merged into one major crack in the middle of the test beam at failure, while L121S084F300 had only one major crack. The reason was that increasing steel fiber content improved the "bridging effect" between the concrete matrix, which was conducive to promote stress redistribution and resist crack instability expansion. There was no spalling for surface concrete of UHPC beams during the failure. The failure of the UHPC beams was completely controlled by the yield of reinforcement and the oblique concrete crushing, which was different from the ordinary concrete beam [18].

This paper took L164S084F075 as an example to describe the failure process of the UHPC beams, as illustrated in Fig. 6(d). The deformation of the UHPC beam under the load was slight and negligible before cracking. The torque was 7.59 kN· m when the first
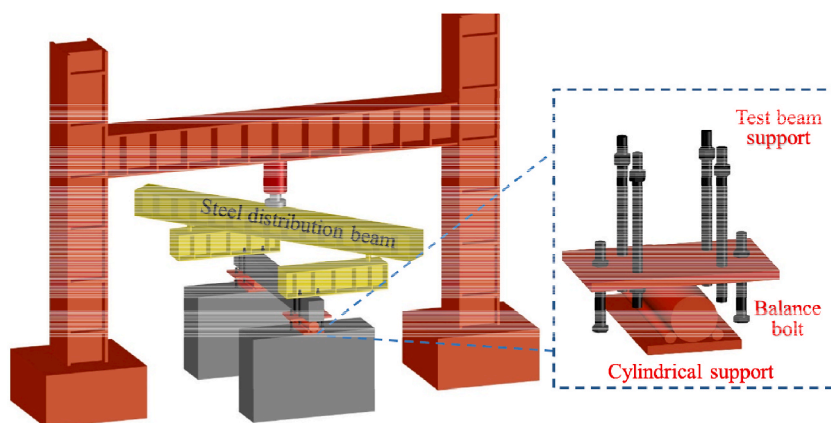
(a)

(b)

Fig. 5. Details of test setup; (a) schematic test setup, (b) actual test setup.

oblique crack appeared in the middle of the side of the UHPC beam, and the crack was slightly invisible. The appearance of crack was accompanied by the obviously sound of "clunk", and the angle between the initial crack and the beam axis was about 45°. As the load increasing, the elongated cracks parallel to the initial cracks kept appearing, and the oblique cracks continually developed to the top and bottom of the UHPC beam. Cracks appeared at the top and bottom of the UHPC beam, as the torque reaching 9.52 kN· m (0.45 T_u). With the increase of load, the oblique cracks continued to expand to the inside of the beam, and finally formed spiral cracks on the surface of the UHPC beam. When torque reached approximately 0.8 T_u, new cracks hardly appeared. The crack width increased with increasing torque. A crack width rapidly increased and continuously merged with surrounding cracks to form a main crack when the torque reached 19.28 kN · m (0.9T_u). With the increase of the load, all the steel fibers on the crack surface were pulled out. The UHPC beam reached ultimate torque (T_u) and was damaged.

4. Experimental results and discussion

4.1. Strain gauge results

The torque - strain curve of the test beams is plotted by selecting the larger strain of the reinforcement at the same torque, as shown in Fig. 7. Before cracking, the slope of the concrete torque-strain curve was significantly smaller than that of the steel torque-strain curve, which indicated that the torque was mainly borne by the concrete. The steel rebar was in an unstressed state at this stage. After cracking, with increased steel fiber content from 0.75% to 1.5% and 3%,the average tensile strains in the concrete on the surface of the UHPC beams were 151 $\mu\varepsilon$, 202 $\mu\varepsilon$, and 234 $\mu\varepsilon$, respectively. The average strain change of reinforcement was less than 30 $\mu\varepsilon$.

As illustrated in Fig. 7(a), the concrete strain showed linear relationship with the torque before cracking. This implies that the concrete was in an elastic state before cracking. Failure occurred rapidly of plain concrete beam after cracking. The plain concrete beam was damaged with only one diagonal crack, leading to not reach the maximum tensile strain in the concrete at the strain gauge attachment. Rapid yielding of the longitudinal bars after cracking caused failure. Compared to the plain concrete beam, several cracks
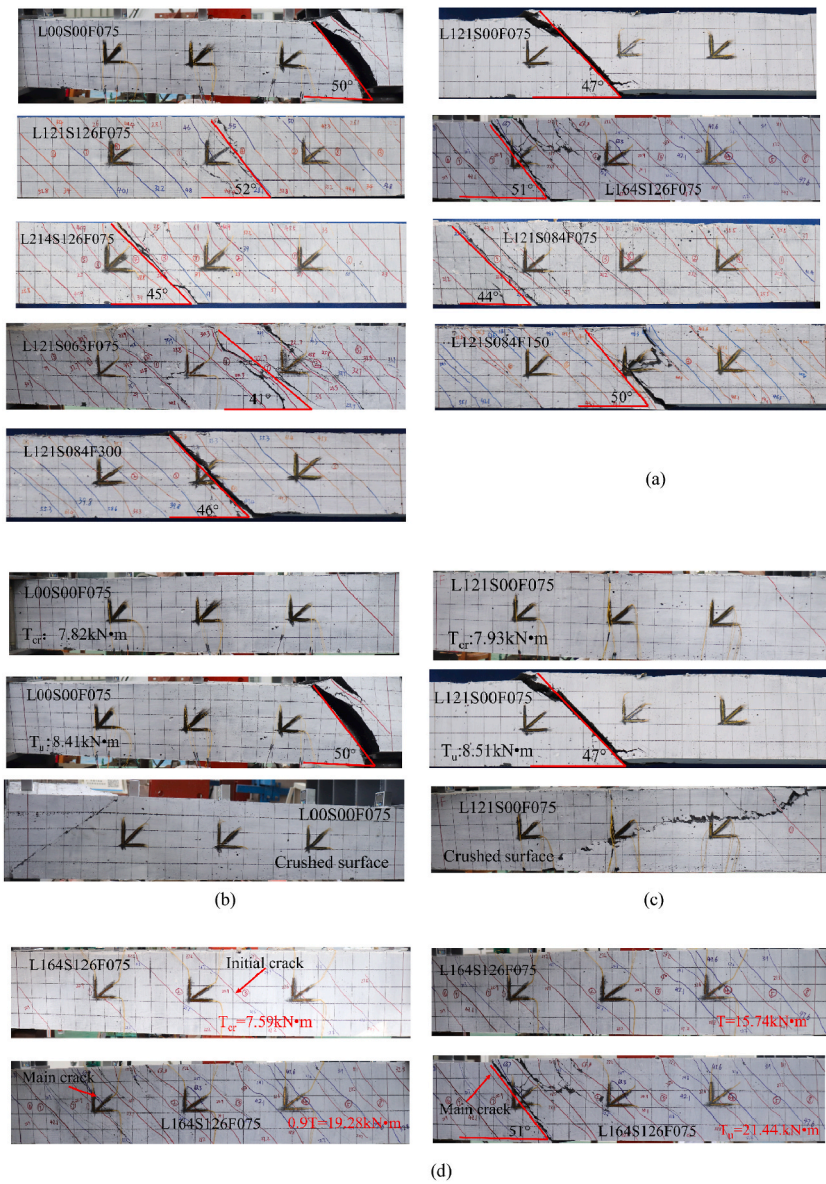
Fig. 6. Failure modes; (a) Test beam failure figure, (b) L00S00F075, (c) L121S00F075, (d) L164S126F075.

appeared on the surface of the UHPC beam with only longitudinal reinforcements. The concrete strain gauges at the cracks fracture leading to a sudden change in concrete strain after cracking. The stirrup yielded first compared to the longitudinal reinforcement.

4.2. Analysis of cracks

Fig. 8(a) shows the torque-main crack width curve. With the increase of crack width, the steel fibers at the crack were gradually pulled out. According to GB50010-2010 [24], the crack width under normal service conditions was limited to 0.3 mm. The crack development was divided into three stages according to the crack width: normal service stage, stable development stage, and instability stage. During the normal service stage (concrete cracking up to 0.3 mm), new cracks were continuously added to the surface with the increase of torque, and several cracks developed simultaneously. The crack width developed slowly and each crack width was similar. The main crack could not be identified. In the stable development stage (the crack width was 0.3 mm to the main crack appeared), the crack width increased obviously after each load, which eventually developed into the main crack. The maximum crack width was basically linear with the torque. The cracks entered the instability stage quickly after the appearance of the main crack. Steel fibers were completely pulled out at the cracks. The crack width increased sharply with the increase of torque, and the maximum crack width was between 10 and 20 mm when the UHPC beams were damaged.

Fig. 8(b) shows the torque-maximum crack width curves for different longitudinal reinforcement ratios. The influence of
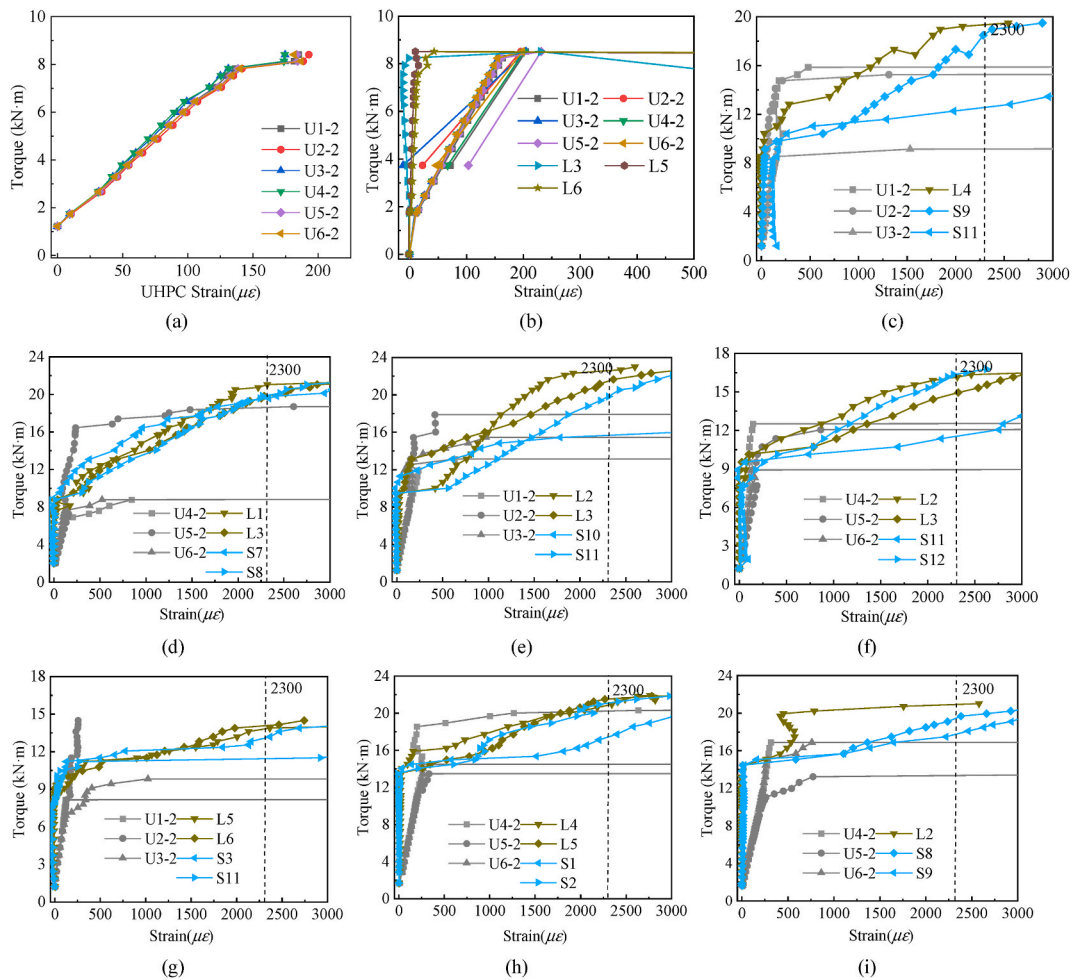
Fig. 7. Torque-strain curve; (a)L00S00F075, (b)L121S00F075, (c)L121S126F075, (d)L164S126F075, (e)L214S126F075, (f)L121S084F075, (g)L121S063F075, (h) L121S084F150, (i)L121S084F300.

longitudinal reinforcement ratio on crack width was different from stirrup ratio. During the normal service stage, the longitudinal reinforcement ratio had little influence on the maximum crack width. The reason was that the cracks under the torque firstly appeared at the midpoint of the long side of the beam section, while the longitudinal reinforcements were configured at the corners of the section to restrain the cracks weakly. After the maximum crack width exceeded 0.3 mm, the maximum crack width decreased with increasing longitudinal reinforcement ratio at the same torque. Because at this time the crack had developed from the middle of the long side of the section to the edge of the section. Fig. 8 (c) shows the torque-maximum crack width curves under different stirrup ratios. The maximum crack width decreased with the increase of the stirrup ratio at the same torque. Because oblique cracks on the surface intersected with the stirrups. The more densely the stirrups resulted in the better the suppression effect on the crack development after cracking.

Fig. 8 (d) shows the torque-maximum crack width curves for different steel fiber contents. The maximum crack width of the UHPC beams with the same reinforcement ratio was significantly reduced with increasing the steel fiber content from 0.75% to 1.5% at the same torque. This means that the crack resistance was effectively improved with the increase of steel fiber contents. However, the maximum crack width of the UHPC beams with the same reinforcement ratio and same torque was similar when the steel fiber admixture was increased from 1.5% to 3%. The reason is that the mechanical properties of 1.5% and 3% UHPC were similar.

Fig. 6 (a) shows the failure mode of UHPC beams. With the same steel fibers content, the number of cracks in the UHPC beams at failure was similar with the increase of longitudinal reinforcement ratio at the same stirrup ratio. The number of cracks at the same longitudinal reinforcement ratio increased with the increase of the stirrup ratio and steel fiber content. This indicates that increasing the stirrup ratio and steel fiber content could effectively enhance the stress redistribution, inhibiting the development of crack width and promoting the multiple cracking behavior. Although the stirrup ratio and steel fiber content had similarly effects, two factors had different ways of action. Increasing the stirrup ratio better transferred torque from the concrete to the test beam, reducing the stress level in the concrete. However, increasing steel fiber content increased the "bridging effect" in concrete, which better eliminated the stress concentration in concrete matrix and inhibited the development of crack width to promote the multiple cracking.
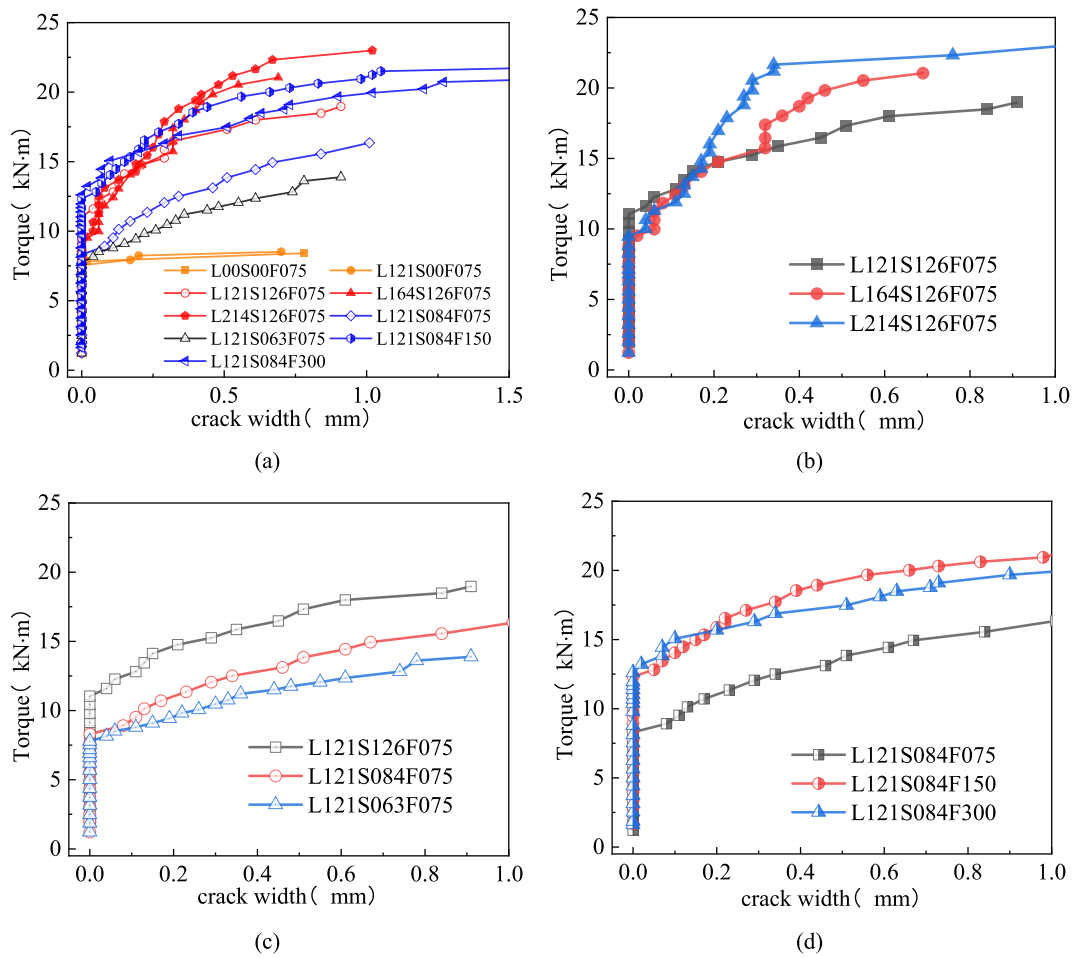
Fig. 8. Effects of test parameters on maximum crack width; (a) Torque-maximum crack width curve, (b) longitudinal reinforcement ratio, (c) stirrup reinforcement ratio, (d) steel fiber content.

4.3. Ductility

The plastic deformation capacity of the UHPC beams is expressed by the torsional ductility index (μ). In this study, the method proposed by Bernardo and Lopes [25,26] was used to calculate the torsional ductility index of the UHPC beams (refer to Eq. (1)), and the results are shown in Table 6.

$$\mu = \frac{\theta_u}{\theta_y} \tag{1}$$

Table 6
Summary of experimental results.

Test beams	T_{cr} (kN·m)	θ_{cr} (rad·m^{-1})	T_y (kN·m)	θ_y (rad·m^{-1})	T_u (kN·m)	θ_u (rad·m^{-1})	μ	K_1 (kN·m^2/rad)	K_2 (kN·m^2/rad)
L00S00F075	7.82	0.0029	–	–	8.41	0.0080	–	2697	134.09
L121S00F075	7.93	0.0029	–	–	8.51	0.0080	–	2734	113.73
L121S126F075	8.54	0.0022	16.33	0.0356	19.49	0.0887	2.49	3882	233.32
L164S126F075	7.59	0.0022	18.65	0.0478	21.44	0.0909	1.90	3450	242.56
L214S126F075	8.24	0.0022	20.74	0.0526	23.00	0.0953	1.81	3745	248.02
L121S084F075	7.69	0.0029	14.69	0.0469	16.50	0.0829	1.77	2652	158.99
L121S063F075	7.53	0.0029	12.69	0.049	14.15	0.0750	1.53	2597	111.89
L121S084F150	11.10	0.0036	19.07	0.0462	21.90	0.0916	1.98	3083	187.16
L121S084F300	11.96	0.0036	19.40	0.0360	22.33	0.0909	2.53	3322	229.57

Where: T_{cr} is cracking torque, θ_{cr} is cracking twist, T_y is yield torque, θ_y is yield twist, T_u ultimate torque, θ_u is ultimate twist, μ is torsional ductility coefficient, K_1 is elastic stiffness, K_2 is plastic stiffness.

Where: μ is torsional ductility index, θ_u is ultimate twist, θ_y is yielding twist.

L00S00F075 and L121S00F075 were brittle failure without calculating the ductility factor. Fig. 9(a) shows the effect of longitudinal reinforcement ratio on the ductility index of the UHPC beam. With the same stirrup ratio, the longitudinal reinforcement ratio increased from 1.21% to 1.64% and 2.14%, the ductility index decreased by 24% and 27%, respectively. The torsional ductility decreased with increasing the longitudinal reinforcement ratio. The reason was that the compressive strength of the concrete at the compression surface was the same when the test beam was damaged, and the higher the longitudinal reinforcement ratio led to the smaller the required deformation of the reinforcement after yielding of reinforcement. Fig. 9(b) illustrates the effect of stirrups ratio on the ductility index. With the same longitudinal reinforcement ratio, the stirrup ratio increased from 0.63% to 0.84% and 1.26%, the ductility index increased by 16% and 63%, respectively. The ductility index increased significantly with the increase of the stirrup ratio. Because the larger the stirrup ratio led to the more adequate the internal force redistribution. Thus, the average crack spacing and crack width on the surface of the test beam was smaller, which made the overall larger deformation before the crack instability damaged.

Fig. 9(c) shows the effect of steel fiber content on the ductility index. With the same reinforcement ratio, the steel fiber content increased from 0.75% to 1.5% and 3%, the ductility index increased by 12% and 43%, respectively. The ductility was increased with the increase of steel fiber content. The reason was that the increase of steel fiber content improved the level of plastic development of concrete, which increased the ultimate twist of the UHPC beams.

4.4. Stiffness and torque-twist curves

The torque-twist curve of the test beams was divided into elastic stage, plastic stage, and failure state. Fig. 10(a) shows the schematic diagram of the stiffness analysis of the UHPC beams.

In the elastic stage, the torque-twist curve was linear before cracking. The stiffness of the UHPC beams was large as shown in Fig. 10 (a) (OA section). The torque-twist curve entered the plastic stage (AB section) after cracking.

In the plastic stage, the torque-twist curve was nonlinear, and the tangent slope of the torque-twist curve declined consistently. The stiffness of UHPC beams was consistently degraded. The yield of the reinforcement was the failure stage (BC section) and the stiffness was further degraded.

The test results for the nine UHPC beams are listed in Table 6. The torsional stiffness of the UHPC beams in elastic and plastic stages was calculated according to eqs. (2) and (3):

$$K_1 = \frac{T_{cr}}{\theta_{cr}} \tag{2}$$

$$K_2 = \frac{T_y - T_{cr}}{\theta_y - \theta_{cr}} \tag{3}$$

The elastic stiffness (K_1) was larger and the reinforcement had less effect on the elastic stiffness before cracking. The K_1 increased with the increase of steel fiber content. The stiffness of the UHPC beam was reduced substantially after cracking. The plastic stiffness was about 1/25–1/10 of K_1. The stiffness decline was similar to that of ordinary concrete beams [5]. Fig. 10(b), (c) and (d) show the effects of longitudinal reinforcement ratio, stirrup ratio and steel fiber content on the plastic stiffness of the UHPC beams, respectively. In the plastic stage, the stiffness of the UHPC beams improved slightly with the increase of the longitudinal reinforcement ratio. However, the stirrup ratio was increased from 0.63% to 0.84% and 1.26%, the stiffness was improved by 42% and 109% respectively. The reason was that the stirrups had a greater limiting effect on the crack width than the longitudinal reinforcement in the plastic stage. The stiffness increased by 18% and 44%, respectively, when the steel fiber content was increased from 0.75% to 1.5% and 3%. The reason was that the steel fibers were not completely pulled out from the concrete matrix at this stage, and the UHPC connected by the steel reinforcement and steel fibers appeared "pseudo strain hardening" phenomenon [27,28]. The increase of steel fiber content improved the tangential modulus of UHPC during "pseudo-strain hardening" [29], which eventually led to the higher stiffness of the UHPC beams.

The torque-twist curve of the test beam is shown in Fig. 11. The twist increased with the decrease of the longitudinal reinforcement
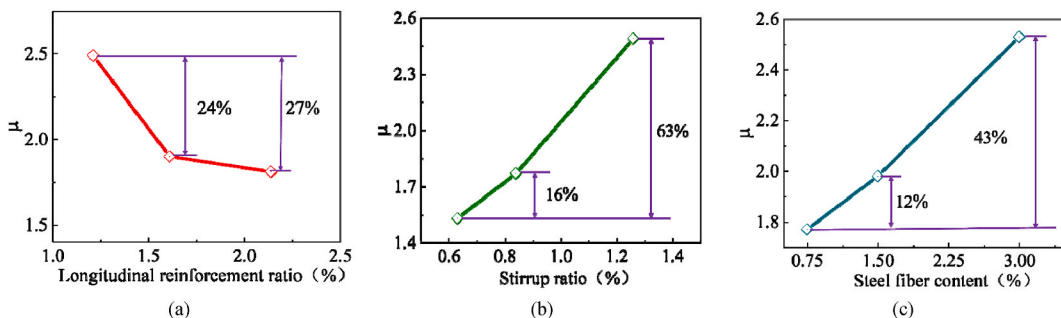

Fig. 9. Effects of test parameters on torsional ductility; (a) longitudinal reinforcement ratio, (b) stirrup reinforcement ratio, (c) steel fiber content.
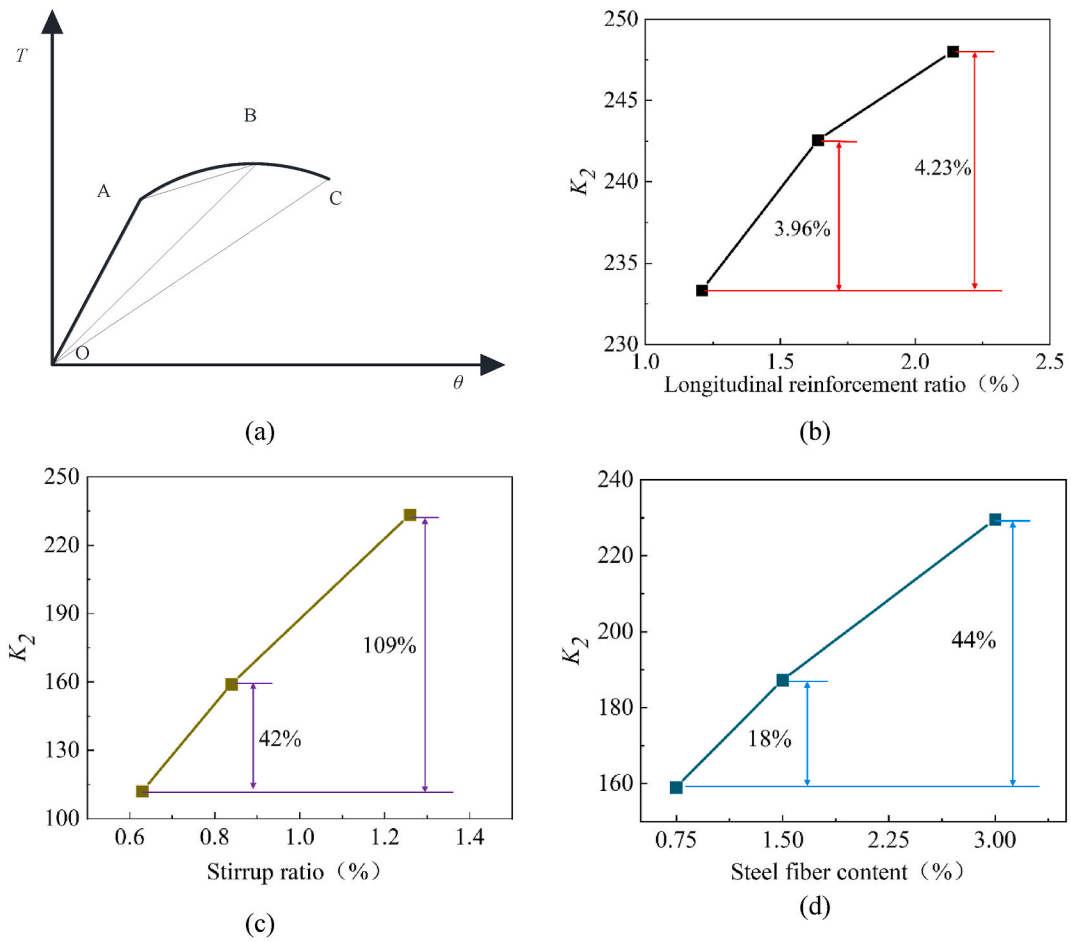
Fig. 10. Effects of test parameters on plastic stiffness; (a) schematic diagram of stiffness analysis, (b) longitudinal reinforcement ratio, (c) stirrup reinforcement ratio, (d) steel fiber content.

ratio and stirrup ratio at the same torque in the plastic stage. The UHPC beam was cracked and the torque was carried by the reinforcement and UHPC. The elastic modulus of reinforcement was larger than that of UHPC, which made the UHPC beams with high reinforcement ratio have greater bearing capacity and stiffness. Moreover, the influence of stirrup ratio on torque-twist curve was more obvious, which was consistent with the influence of reinforcement ratio on the stiffness. At the same torque, the twist decreased with
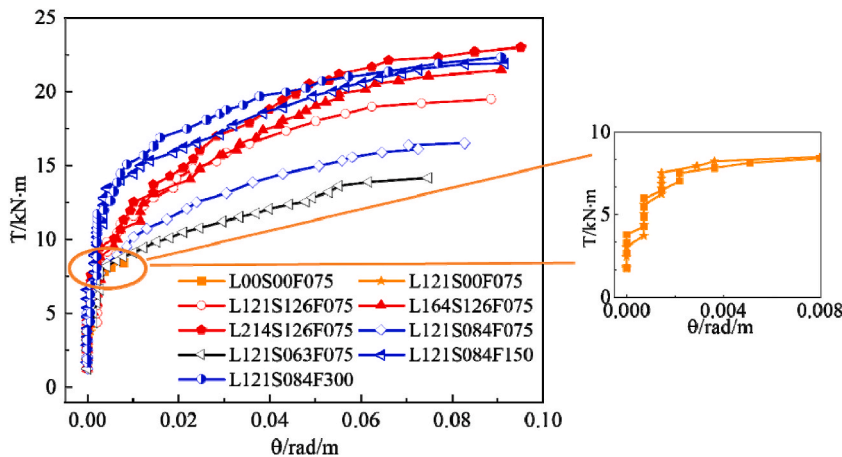

Fig. 11. Torque-twist curve.

the increase of steel fiber content. This implies that the increase of steel fiber content improved the tensile strength of the concrete and restrained the development of the crack width, resulting in reducing deformation of the test beams. The UHPC beams entered the failure stage when the ultimate torque was approached. The torque raise was small with the increase twist of the UHPC beam.

4.5. Load capacity analysis

The cracking torque of the UHPC beams is depicted in Fig. 12(a). The influence of longitudinal reinforcement ratio and stirrup ratio on cracking torque was small. Before cracking, torque was mainly borne by concrete. The elastic modulus of reinforcement was greater than that of UHPC. The placement of reinforcement in concrete increased the strength of the UHPC beams, meanwhile the presence of reinforcement increased the weak cross section of the UHPC beams, and the two superimposed on each other affected the cracking torque.

The influence of steel fiber content on the cracking torque is depicted in Fig. 12(b). The cracking torque increased by 44% and 56% respectively when the steel fiber content was increased from 0.75% to 1.5% and 3%. The reason was that the "bridging effect" in the concrete matrix was enhanced with the increase of steel fiber content. Increasing tensile strength of the concrete led to improve the cracking torque. However, the cracking torque was improved by 8% when the steel fiber content was increased from 1.5% to 3%. This implies that the stress concentration [29] inside the concrete was caused by the agglomerate together form clusters of steel fibers in the concrete when the steel fiber content was too large. The tensile strength of the concrete was increased thus the cracking torque of the test beam was improved.

The ultimate torque of each UHPC beams was compared, as illustrated in Fig. 13(a). The ultimate torque of L121S00F075 was improved 1.2% compared to L00S00F075, which indicated that only the longitudinal reinforcement had not significant effect on the ultimate torque. The effects of longitudinal reinforcement ratio and stirrups ratio on the ultimate torque are illustrated in Fig. 13(b) and (c). With the same stirrup ratio and steel fiber content, the ultimate torque was improved by 10% and 18% when the longitudinal reinforcement ratio was increased from 1.21% to 1.64% and 2.14%, respectively. At the same longitudinal reinforcement ratio and steel fiber content, the ultimate torque was improved by 16% and 34% when the stirrup ratio was increased from 0.63% to 0.84% and 1.26%, respectively. The tensile strength of the reinforcement was greater than the tensile strength of the concrete that increasing the reinforcement ratio could effectively improve the ultimate load capacity. Moreover, the effect of stirrup ratio on the ultimate torque was greater compared to the longitudinal reinforcement ratio, similar as the finding from Yang [16].

The influence of steel fiber content on the ultimate torque is depicted in Fig. 13(d). At the same reinforcement ratio, the ultimate torque was improved by 30.5% and 33.1% with increasing the steel fiber content from 0.75% to 1.5% and 3%, respectively, but the ultimate torque was improved by only 2% with increasing the steel fiber content from 1.5% to 3%. The reason was that the splitting tensile strength of UHPC was highest at 2% of steel fiber content [30]. This indicated that the ultimate load capacity of the UHPC beam was effectively improved with increasing steel fiber content or the reinforcement ratio at a reasonable reinforcement strength ratio.

4.6. Energy dissipation and damage

The process of twisting concrete beams was accompanied by energy dissipation and damage. In this paper, energy method of the Najar [31,32] was used to study the torsional damage of UHPC beams. The complete torque-twist curve of the UHPC beams is illustrated in Fig. 14. The straight line OD represented the non-destructive loading route of the UHPC beams in the ideal state, the work of the external force in the ideal state:

$$W = S_{ODA} = K\theta^2/2 = W_E + W_P + W_D \tag{4}$$

The curve OCB is the actual loading curve of the damage, and the area of the region OCBA is the deformation energy of the test beam, and the actual work done by the external force is:

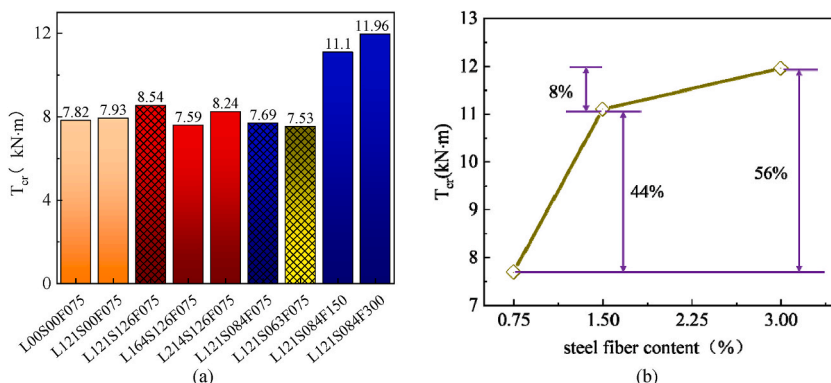$$S_{OCBA} = W_E + W_P \tag{5}$$

Fig. 12. Cacking torques; (a) comparison of cracking torque, (b) cracking torque of different steel fiber content.
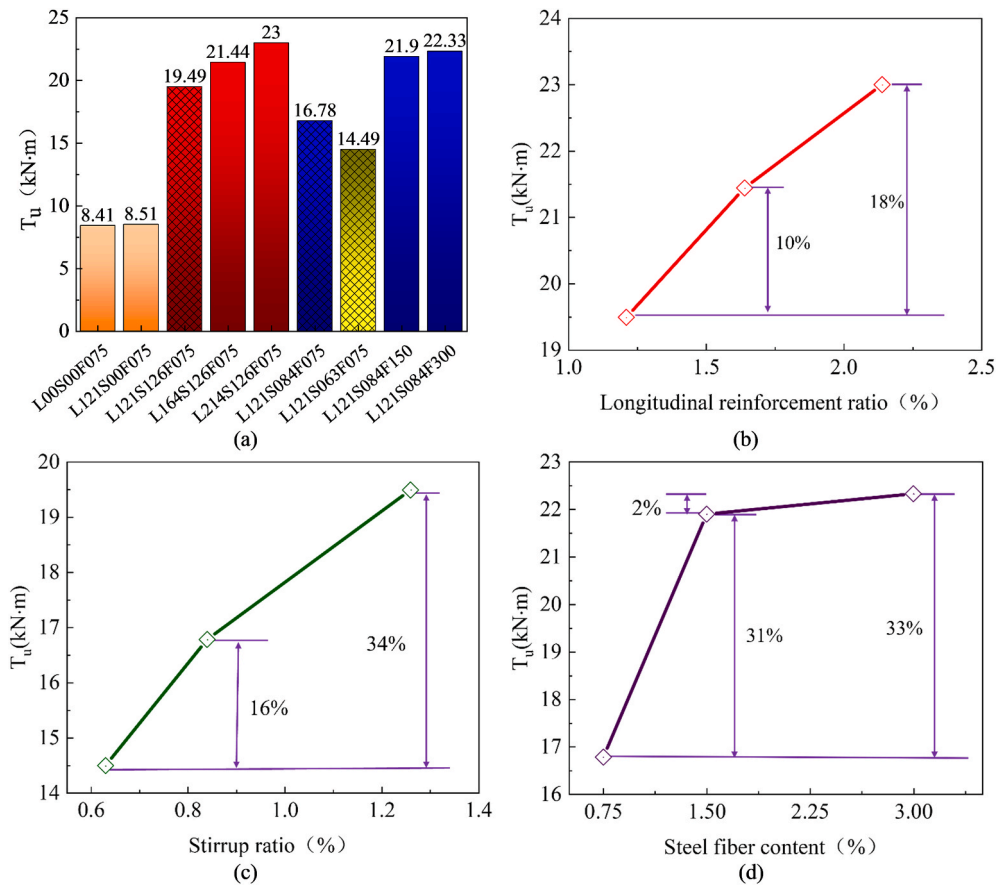
Fig. 13. Ultimate torque; (a) comparison of ultimate torque, (b) Longitudinal reinforcement ratio, (c) Stirrup reinforcement ratio, (d) Steel fiber content.
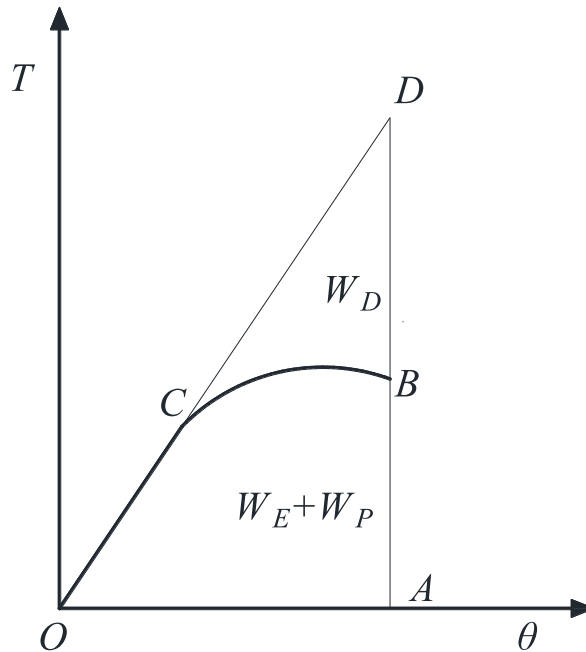

Fig. 14. Whole process curve of torque-twist.

Where: W is the work done by the external force in the ideal state; K is the average stiffness of the test beam before cracking and the value is equal to K_1; θ is the twist of the test beam at the time of failure; W_E is the elastic deformation energy; W_P is the plastic deformation energy; W_D is damage energy dissipation.

The energy consumption capacity of the UHPC beam during torsion is denoted by the energy dissipation coefficient β. D is the damage index.

$$\beta = \frac{W_E + W_P}{W} \tag{6}$$

$$D = \frac{W_D}{W} = 1 - \beta \tag{7}$$

The energy dissipation coefficient and damage index of each UHPC beams are listed in Table 7. The damage index ranged from 0.85 to 0.90. The energy dissipation ($W_E + W_P$) improved with the increase of reinforcement ratio and steel fiber content. The reason was that the elastic modulus of reinforcement kN and steel fiber was greater than that of UHPC, and the increase of reinforcement ratio and steel fiber content made the UHPC beam require more external work during the failure. However, the damage indexes of the test beams were similar. Because the plastic stiffness of the UHPC beams was much smaller than the elastic stiffness, resulting in too much numerical disparity between the energy dissipated in each UHPC beam and the work done by the external force in the ideal state of the UHPC beam.

5. Formula to calculate the torsional capacity of UHPC beams

5.1. Cracking torque

In this paper, the calculation methods recommended by ACI 318–19 [33], GB50010-2010 [24] and Kwahk [34] were used to calculate the cracking torque of the UHPC beams. The calculation equations are shown in Table 8. ACI 318–19 [32] and Kwahk [34] were based on thin-walled tube theory to derive the formula for cracking torque. GB50010-2010 [24] was based on the plasticity theory to derive the cracking torque of reinforced concrete beams under the action of pure torsion. The level of plastic development of the cross-section and the biaxial stress intensity criterion were considered in the derivation process.

The theoretical values and test values of the suggestion formula for cracking torque are listed in Table 9 and Fig. 15. The influence of reinforcement on cracking torque was neglected in the derivation of each formula. The average values of the ratios of the test values to the theoretical values of GB50010-2010 [24], ACI318-19 [33] and Kwahk [34] suggestion formula were 1.14, 1.37 and 0.96, respectively, with corresponding coefficients of variation of 9%, 15% and 9%. GB50010-2010 [24] and ACI318-19 [33] were conservative prediction for cracking torque of UHPC beams. It has a certain safety reserve in the actual engineering application. The reason was that GB50010-2010 [24] was derived from the empirical data of ordinary concrete beams, while UHPC beams had a greater level of plastic development during torsion than ordinary concrete beams. ACI 318–19 [33] was more conservative prediction for cracking torque when the steel fiber content was changed. Because ACI 318–19 [33] converted the compressive strength of concrete to calculate the cracking torque, and the increase of steel fiber content had a more significant effect on the tensile strength of concrete compared to the compressive strength of concrete. The theoretical value of Kwahk [34] was closest to the test value, but Kwahk [34] was slightly unconservative prediction for cracking torque, which was dangerous in the actual engineering application.

Kwahk [34] provided a good prediction for UHPC with 0.75% steel fiber, but the prediction became worse when the steel fiber volume increases. GB50010-2010 [24] on the other hand given a better prediction based on fiber content. The maximum tensile stress on the concrete in a rectangular UHPC beams in torsion was at the midpoint of the long side of the section, i.e. the UHPC beams cracked from the midpoint of the side. The greater the tensile strength of the concrete, the further the actual tensile stresses in the concrete above and below the test beam were from the maximum tensile strength at the time of cracking, resulted in a waste of the tensile strength of the concrete. The formula provided in GB50010-2010 [24] included a factor W_t for the form of the test beam section. Therefore, the difference between the predicted and actual values of GB50010-2010 [24] varies less with the increased in tensile strength. In contrast, Kwahk prediction formula did not contain this type of factor.

5.2. Ultimate torsional capacity

5.2.1. Derivation and comparison of calculation formulas

The formulas recommended by ACI 318–19 [33], GB50010-2010 [24] and the formulas derived by space truss model with

Table 7
Energy dissipation coefficient and damage index of the test beam.

Test beams	$W/(\text{kN} \cdot \text{m}^2)$	$W_E + W_P/(\text{kN} \cdot \text{m}^2)$	β	D
L121S126F075	15.270	1.633	0.107	0.893
L164S126F075	14.253	1.554	0.109	0.891
L214S126F075	17.008	1.767	0.104	0.896
L121S084F075	9.112	1.120	0.123	0.877
L121S063F075	7.303	0.863	0.118	0.882
L121S084F150	12.935	1.697	0.131	0.869
L121S084F300	13.725	1.736	0.127	0.873

Table 8

Cracking torque calculation formula.

Calculation methods	Equation
ACI318-19	$T_{cr} = 0.33 \frac{A_c}{P_c} \sqrt{f_c}$
GB50010-2010	$T_{cr} = 0.7 f_t W_t,\ W_t = \frac{b^2 (3h - b)}{6}$
Kwahk	$T_{cr} = 2 A_0 f_t t,\ t = t_{ef}$

Where: A_c is area of the cross section, P_c is perimeter of the cross section, f_c is compressive strength of concrete cubes, f_t is tensile strength of concrete, W_t is torsional plastic resistance moment of the cross section, b is section width, h is section height, A_0 is area limited by the center-line of shear flow, t_{ef} is equivalent thickness of thin wall.

Table 9

Comparison of cracking torque test values and theoretical values.

Test beams	$T_{cr,Exp}$ (kN · m)	$T_{cr,Pred}$ (kN · m)			$T_{cr,Exp}/T_{cr,Pred}$		
		GB50010	ACI	Kwahk	GB50010	ACI	Kwahk
L00S00F075	8.54	6.65	6.25	7.91	1.28	1.37	1.08
L121S00F075	7.59	6.65	6.25	7.91	1.14	1.21	0.96
L121S126F075	8.24	6.65	6.25	7.91	1.24	1.32	1.04
L164S126F075	7.69	6.65	6.25	7.91	1.16	1.23	0.97
L214S126F075	7.53	6.65	6.25	7.91	1.13	1.20	0.95
L121S084F075	7.82	6.65	6.25	7.91	1.18	1.25	0.99
L121S063F075	7.93	6.65	6.25	7.91	1.19	1.27	1.00
L121S084F150	11.10	11.18	6.45	13.31	0.99	1.72	0.83
L121S084F300	11.96	12.46	6.65	14.83	0.96	1.80	0.81
average value					1.14	1.37	0.96
Variance					0.10	0.21	0.08
COV					9%	15%	9%

Where: $T_{cr,Exp}$ is the test value of cracking torque, $T_{cr,Pred}$ is the cracking torque prediction, ACI is ACI318–19, GB50010 is GB50010-2010.
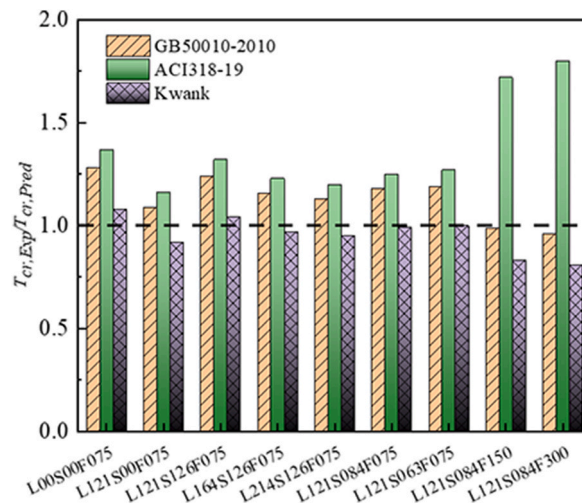

Fig. 15. Theoretical-to-experimental T_{cr} ratio.

thin-walled tube model were used to predict the ultimate torque of the UHPC beams, as listed in Table 10. ACI318-19 [33] simplified the concrete beam using the space truss model and neglected the role of concrete in the torsion process to derive the ultimate torque calculation formula. GB50010-2010 [24] based on plasticity theory would be many test data for statistical regression to derive the ultimate torque calculation formula. In the formula, the contribution of concrete and reinforcement to the ultimate torque were included.

Calculation of torsional ultimate load capacity of UHPC beams based on space truss theory [35] and thin-walled management theory [34]. The torsional load bearing capacity of UHPC beams consisted of two parts: reinforcement and concrete. The torsional load capacity of the reinforcement was recorded as T_1 in accordance with the space truss model, as shown in Fig. 16.

Table 10

Ultimate torque calculation formula.

Calculation methods	Equation
ACI318-19	$T_n = \min\left\{\dfrac{2A_0A_{sv1}f_{yv}}{s}\cot\theta, \dfrac{2A_0A_{sl}f_{yl}}{p_h}\cot\theta\right\}$
GB50010-2010	$T_n = 0.7f_tW_t + 1.2\sqrt{\zeta}\,\dfrac{f_{yv}A_{sv1}A_{cor}}{s}, \zeta = \dfrac{f_{yl}A_{sl}s}{f_{yv}A_{sv1}u_{cor}}, W_t = \dfrac{b^2(3h-b)}{6}$
Eq. 22	$T = T_1 + T_2 = 2\sqrt{\zeta}\,\dfrac{A_{sv1}f_{yv}A_{cor}}{s} + 2f_tA_{cor}t\cot\theta$

Where: A_0 is area limited by the center-line of shear flow, A_{sv1} is area of single leg of stirrups, A_{sl} is total area of longitudinal reinforcement, θ is angle of compression struts, $30° \leq \theta \leq 60°$, f_{yl} is yield strength of longitudinal reinforcement, f_{yv} is yield strength of stirrup, s is spacing of stirrups, p_h is perimeter of centerline of outermost closed stirrups, ζ is ratio of longitudinal reinforcement to stirrups, A_{cor} is area enclosed by inner surface of stirrup, t is effective wall thickness.

In the variable angle space truss model, the internal forces of the longitudinal reinforcement chord, the stirrup web and the concrete strut were represented by P, Q and R respectively. The component forces of the internal force R in the X and Y directions were balanced with Q, and the component forces in the Z direction were balanced with P.

The shear flow in the cross-section of a reinforced concrete member was balanced by the torque:

$$T_1 = (qh_{cor}b_{cor} + qb_{cor}h_{cor}) = 2qA_{cor} \tag{8}$$

A complete oblique crack was taken as the isolator.

$$Q = qh_{cor} = \frac{A_{sv1}f_{yv}h_{cor}\cot\theta}{s} \tag{9}$$

$$q = \frac{A_{sv1}f_{yv}\cot\theta}{s} \tag{10}$$

By the equilibrium condition we got:

$$P = Q\cot\theta \tag{11}$$

$$A_{sl}f_{yl}\frac{h_{cor}}{u_{cor}} = qh_{cor}\cot\theta \tag{12}$$

$$\cot\theta = \frac{A_{sl}f_{yl}}{qu_{cor}} \tag{13}$$

Substituting Eq. (13) into Eq. (10) given:

$$q = \sqrt{\frac{A_{sv1}f_{yv}}{s}\frac{A_{sl}f_{yl}}{u_{cor}}} \tag{14}$$

ζ was the reinforcement strength ratio of longitudinal reinforcement and stirrup of torsion member.

$$\tan\theta = \sqrt{\frac{A_{sv1}f_{yv}u_{cor}}{A_{sl}f_{yt}s}} = \sqrt{\frac{1}{\zeta}} \tag{15}$$

$$\zeta = \frac{A_{sl}f_{yl}s}{A_{sv1}f_{yv}u_{cor}} \tag{16}$$

Substituting Eq. (14) and Eq. (16) into Eq. (8) yields:

$$T_1 = 2\sqrt{\zeta}\,\frac{A_{sv1}f_{yv}A_{cor}}{s} \tag{17}$$

The torsional load bearing capacity of concrete was recorded as T_2. As shown in Fig. 17, the tensile force of concrete at the crack was balanced by the shear flow and longitudinal reinforcement tension, respectively.

$$T_2 = F_1b_{cor} + F_2h_{cor} \tag{18}$$

$$\frac{f_th_{cor}t}{\sin\theta}\cos\theta = F_1 \tag{19}$$

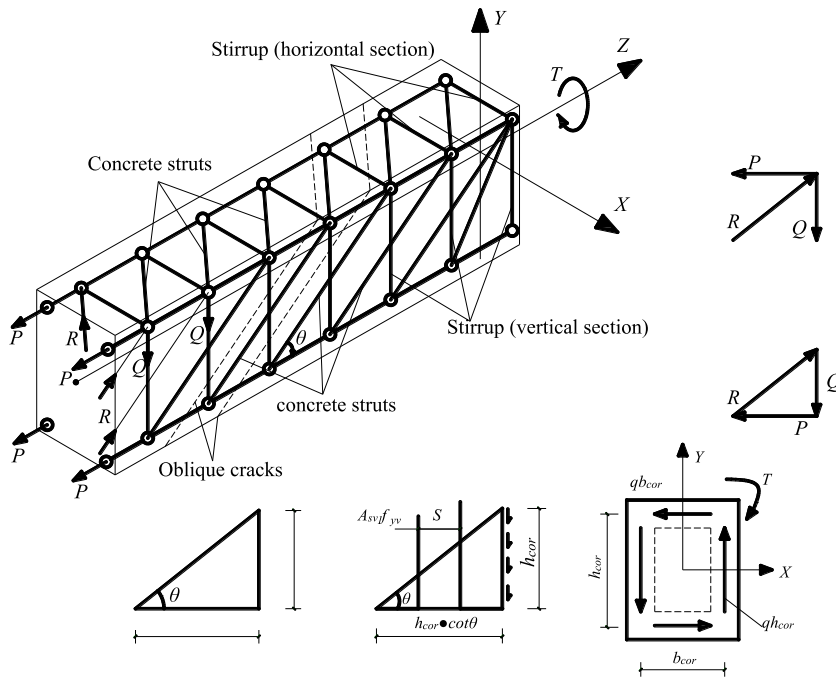$$\frac{f_tb_{cor}t}{\sin\theta}\cos\theta = F_2 \tag{20}$$

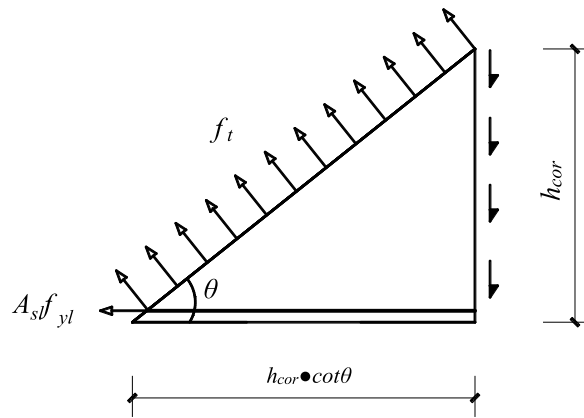**Fig. 16.** Stress analysis diagram of space truss model.

Fig. 17. Stress analysis diagram of thin-walled tube model.

$$T_2 = 2f_t b_{cor} h_{cor} t \cot \theta \tag{21}$$

$$T = T_1 + T_2 = 2\sqrt{\zeta} \, \frac{A_{sv1} f_{yv} A_{cor}}{s} + 2f_t A_{cor} t \cot \theta \tag{22}$$

The theoretical values and test values of the recommended formula for the ultimate torque of the UHPC beam are illustrated in Table 11 and Fig. 18. The average values of the ratios of the test values to the theoretical values of ACI 318–19 [33], GB50010 [24] and Eq. (22) recommended formula were 1.53, 1.77 and 0.79, respectively, and the corresponding coefficients of variation were 18.69%, 3.74% and 7.97%. ACI 318–19 [33] was conservative prediction for the ultimate torque of the UHPC beam. ACI318-19 [33] simplified the test beams into a box type by neglecting the concrete tensile strength, a simplification for ordinary concrete torsional beams. However, this calculation method was not applicable to UHPC beams, and the deviation of the test value from the theoretical value was greater for higher steel fiber content. The reason was that the addition of steel fibers made the tensile strength of UHPC significantly higher than that of ordinary concrete. GB50010-2010 [24] was more conservative prediction for the ultimate torque. GB50010-2010 [24] considered the combined effect of concrete and reinforcement, but the performance of UHPC differed significantly from that of ordinary concrete. The regression expression derived from ordinary concrete tests was inapplicable to reinforced UHPC beams. Eq. (22) overestimated the ultimate torque, but the variance and coefficient of the theoretical values were small. The prediction results

Table 11
Comparison of ultimate torque test values and theoretical values.

Test beams	$T_{u,Exp}$ (kN · m)	$T_{u,Pred}$ (kN · m)			$T_{u,Exp}/T_{u,Pred}$		
		ACI	GB50010	Eq. 22	ACI	GB50010	Eq. 22
L00S00F075	8.54	–	–	–	–	–	–
L121S00F075	7.26	–	–	–	–	–	–
L121S126F075	19.49	13.13	10.83	22.03	1.38	1.80	0.88
L164S126F075	21.44	16.41	12.04	25.58	1.31	1.78	0.84
L214S126F075	23.00	18.63	13.22	29.04	1.23	1.74	0.79
L121S084F075	16.50	11.54	9.45	21.21	1.43	1.75	0.78
L121S063F075	14.15	10.00	8.63	20.16	1.42	1.64	0.67
L121S084F150	21.90	11.54	11.72	27.81	1.90	1.87	0.79
L121S084F300	22.33	11.54	12.36	29.67	1.93	1.81	0.75
average value					1.53	1.77	0.79
Variance					0.28	0.07	0.06
COV					18.69%	3.74%	7.97%

Where: $T_{u,Exp}$ is the test value of ultimate torque; $T_{u,Pred}$ is the ultimate torque prediction.
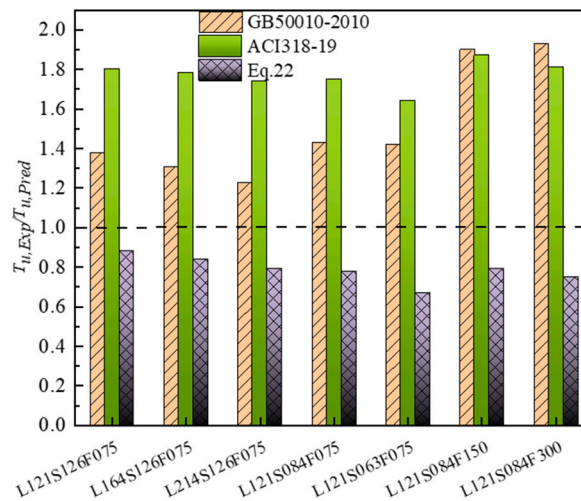

Fig. 18. T_u theoretical-to-experimental T_u ratio.

have a low dispersion.

5.2.2. Optimization of the derivation formula

Eq. (22) of UHPC ultimate torque based on space truss model and thin wall management theory. However, Eq. (22) prediction of the ultimate torque was unconservative. The main reason was to overestimate the effect of concrete on the ultimate torque. The specific reasons are as follows.

(1) Eq. (22) considered the tensile properties of UHPC but the ultimate tensile states of concrete and reinforcement were not simultaneous after cracking.
(2) As the crack width increased, the actual torsional section of the test beam became smaller, which was unconsidered by Eq. (22).
(3) The concrete was under biaxial stress and the actual tensile strength of the concrete was reduced when the test beam was loaded with torque.

Therefore, the concrete torsional reduction coefficient α is proposed to represent the combined effect of the overestimated concrete on the ultimate torque of the test beam due to the above reasons.

Table 12
Comparison between test value and theoretical value with different values of α.

α	0.3	0.4	0.5	0.6	0.7	0.8
average value	1.17	1.07	1.03	0.94	0.89	0.85
Variance	0.10	0.08	0.07	0.06	0.06	0.06
COV	0.09	0.08	0.07	0.06	0.06	0.07

The ultimate torque calculation formula of the UHPC beam is:

$$T_n = 2\sqrt{\zeta}\,\frac{A_{cor}A_{sv1}f_{yv}}{s} + 2\alpha A_{cor}f_t t \cot\theta \tag{23}$$

Table 12 shows the comparison between the test values and the theoretical value of the UHPC beams with different values of α. According to Table 12, the test value is most consistent with the theoretical value at 0.5, with the average value of 1.03, the variance of 0.07 and the coefficient of variation of 0.07.

The comparison of the prediction results of ACI 318–19 [33], GB50010-2010 [24], Eq. (22) and Eq. (23) were shown in Fig. 19. Eq. (23) was used to calculate the ultimate torque for the 14 test beams in the literature [16,20]. As shown in Table 13, the average, variance, and coefficient of variation of the ratio of the ultimate torque test value to the theoretical value are 1.13, 0.17, and 0.15, respectively. This shows that Eq. (23) can better predict the ultimate torsional load capacity of UHPC beams, and the calculated results agree well with the test results. However, the value of the torsional reduction coefficient has certain limitations due to the small number of test beams in this study. More torsional tests on UHPC beams are needed to verify the torsional reduction coefficient values proposed in this study.

6. Conclusions

In this paper, the influence of longitudinal reinforcement ratio, stirrup ratio and steel fiber content on the torsional performance of the nine UHPC beams was investigated. Based on the experimental results and analysis, the following conclusions were demonstrated.

(1) UHPC beams with appropriate longitudinal rebars ratio and stirrups ratio were ductile failure, while UHPC beams with only longitudinal reinforcement were brittle failure. The internal force redistribution of UHPC beams was promoted and the development of crack width was restrained with increasing the stirrup ratio and steel fiber content. During the normal service stage, the longitudinal reinforcement ratio had little influence on the maximum crack width of the UHPC beams. The maximum crack width of UHPC beams with the same torque decreased with the increase of longitudinal reinforcement ratio in the stable development stage and instability stage.

(2) The torsional ductility of UHPC beams decreased with increasing the longitudinal reinforcement ratio, but increased with the increase of the stirrup ratio and steel fiber content.

(3) The reinforcement had less impact on the UHPC beams on the elastic stiffness K_1. Greater steel fiber content results in higher K_1. The plastic stiffness improved with the increase of stirrup ratio and steel fiber content, but the longitudinal reinforcement ratio has little effect on the plastic stiffness of UHPC beams. The plastic stiffness of UHPC beams was approximately 1/25 to 1/10 of the elastic stiffness. The twist of the UHPC beams decreased with the increase of the longitudinal reinforcement ratio, stirrup ratio and steel fiber content at the same torque in the plastic stage.

(4) The reinforcement (longitudinal reinforcement and stirrups) had less effect on the cracking torque of UHPC beams, and the ultimate torque of UHPC beams improved with the increase of reinforcement ratio. The cracking torque and ultimate torque of UHPC beams improved with the increase of steel fiber content, but the cracking torque and ultimate torque of the UHPC beams were slightly improved when the steel fiber content was increased from 1.5% to 3%.

(5) The energy dissipation of UHPC beams was improved with the increase of longitudinal reinforcement ratio, stirrup ratio and steel fiber content. However, the energy dissipation coefficients and damage indexes were similar. The damage index of UHPC beams was between 0.85 and 0.90.
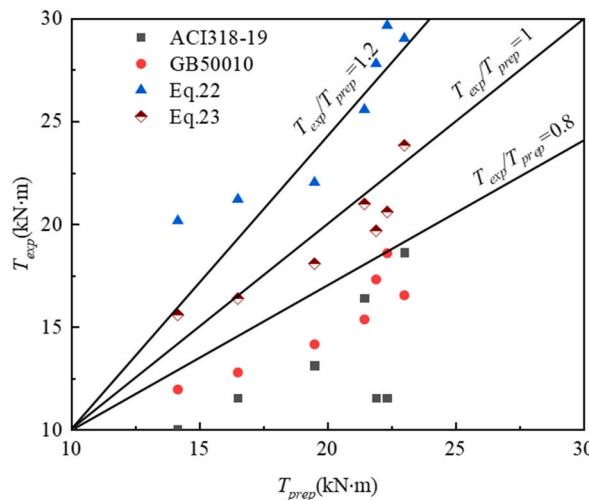

Fig. 19. Comparison of the theoretical results and experimental results.

Table 13
Comparison of test and theoretical values with α as 0.5

References	Test beams	(kN · m)	$T_{Eq.23}$ (kN · m)	$T_{Exp}/T_{Eq.23}$	average value	Variance	COV
This study	L121S126F075	19.49	18.08	1.08	1.03	0.07	0.07
	L164S126F075	21.44	20.99	1.02			
	L214S126F075	23.00	23.84	0.96			
	L121S084F075	16.50	16.38	1.01			
	L121S063F075	14.15	15.58	0.91			
	L121S084F150	21.90	19.68	1.11			
	L121S084F300	22.33	20.60	1.08			
Yang et al. [16]	SS-F1-L56-S35	75.3	64.85	1.16	1.13	0.17	0.15
	SS-F1-L56-S70	86.70	60.63	1.43			
	SS-F2-L56-S35	85.60	105.22	0.81			
	SS-F2-L56-S70	109.80	78.39	1.40			
	SS-F2-L88-S35	114.70	99.67	1.15			
	SS-F2-L88-S70	115.20	88.66	1.30			
	SS-F2-L127-S35	109.60	119.68	0.92			
	SS-F2-L127-S70	119.30	106.22	1.12			
Zhou et al. [20]	HB200T50-1	19.55	20.88	0.94			
	HB200T50-2	21.12	20.88	1.01			
	HB300T80-1	64.11	56.30	1.14			
	HB300T80-2	61.47	56.30	1.09			
	CHB300T50-1	62.27	54.60	1.14			
	CHB300T50-2	63.36	54.60	1.16			

(6) In terms of the prediction of torsional load capacity of UHPC beams, ACI318–19 and GB50010-2010 are more conservative. Based on the spatial truss model, the calculation formula of torsional bearing capacity of rectangular UHPC beams is proposed. Using Eq. (23) of this paper to calculate the torsional load capacity of the literature, the deviation of the literature test value from the theoretical value was small, so the torsional calculation formula of UHPC proposed in this paper was reasonable. However, there are fewer UHPC beams in this study, and more torsional tests of UHPC beams are needed to verify the torsional calculation formula proposed in this study.

CRediT authorship contribution statement

Xia Cao: Conceptualization, Investigation, Methodology, Supervision, Writing – original draft. **Wei-Jia Zhang:** Investigation. **Yi-Cheng Ren:** Investigation. **Feng Fu:** Investigation, Writing – review & editing. **Da-Bo He:** Investigation. **Yan Zheng:** Writing – review & editing.

Declaration of competing interest

The authors declare that they have no known competing financial interests or personal relationships that could have appeared to influence the work reported in this paper.

Data availability

Data will be made available on request.

References

[1] X. Cao, Y.C. Ren, L. Zhang, et al., Flexural behavior of ultra-high performance concrete beams with various types of rebar, Compos. Struct. 292 (2022), 115674.
[2] K. Turker, I.B. Torun, Flexural performance of highly reinforced composite beams with ultra-high- performance fiber reinforced concrete layer, Eng. Struct. 219 (2020), 110722.
[3] Q. Wang, H.L. Song, C.L. Lu, et al., Shear performance of reinforced ultra-high performance concrete rectangular section beams, Structures 27 (8) (2020) 1184–1194.
[4] X. Cao, Y.C. Ren, K. Qian, et al., Size effect on flexural behavior of ultra-high performance concrete beams with different reinforcement, Structures 41 (2022) 969–981.
[5] D.S. Hong, Experimental investigation on rectangle reinforced concrete beams under pure torsion, J. Fuzhou Univ. (2) (1981) 1–28.
[6] S. Lopes, L. Bernardo, Twist behavior of high-strength concrete hollow beams–Formation of plastic hinges along the length, Eng. Struct. 31 (1) (2009) 138–149.
[7] K.N. Rahal, Torsional strength of normal and high strength reinforced concrete beams, Eng. Struct. 56 (2013) 2206–2216.
[8] T.D.G. Rao, D.R. Seshu, Torsion of steel fiber reinforced concrete members, Cement Concr. Res. 33 (11) (2003) 1783–1788.
[9] F. Okay, S. Engin, Torsional behavior of steel fiber reinforced concrete beams, Construct. Build. Mater. 28 (1) (2012) 269–275.

[10] A. Karimipour, J.D. Brito, M. Ghalehnovi, et al., Torsional behaviour of rectangular high-performance fibre-reinforced concrete beams, Structures 35 (2022) 511–519.

[11] F.D. Larrard, T. Sedran, Optimization of ultra-high-performance concrete by the use of a packing model, Cement Concr. Res. 24 (6) (1994) 997–1009.

[12] Y.P. Zhu, Y. Zhang, H.H. Hussein, et al., Flexural strengthening of reinforced concrete beams or slabs using ultra-high-performance concrete (UHPC): a state of the art review, Eng. Struct. 205 (Feb.15) (2020), 110035.1-110035.19.

[13] J.Q. Xue, B. Briseghella, F.Y. Huang, et al., Review of ultra-high-performance concrete and its application in bridge engineering, Construct. Build. Mater. 260 (2020), 119844.

[14] M. Zhou, W. Lu, J. Song, et al., Application of ultra-high performance concrete in bridge engineering, Construct. Build. Mater. 186 (2018) 1256–1267.

[15] D.H. Wang, C.J. Shi, L.M. Wu, Research and applications of ultra-high performance concrete (UHPC) in China, Bull. Chin. Ceram Soc. 35 (1) (2016) 141–149.

[16] I.H. Yang, C. Joh, J.W. Lee, Torsional behavior of ultra-high performance concrete squared beams, Eng. Struct. 56 (2013) 372–383.

[17] A.S. Alamli, H. Mehdi, R. Ahmed, Cracks torque of T section R.C beam with web perforation using reactive powder concrete, Int. J. Civ. Struct. Environ. Infrastruct. Eng. Res. Dev. 6 (2016) 21–28.

[18] M.S. Ibrahim, E. Gebreyouhannes, A. Muhdin, et al., Effect of concrete cover on the pure torsional behavior of reinforced concrete beams - ScienceDirect, Eng. Struct. 216 (2020), 110790.

[19] T.J. Mohammed, B.H. Abu Bakar, N.M. Bunnori, Torsional improvement of reinforced concrete beams using ultra high-performance fiber reinforced concrete (UHPFC) jackets – experimental study, Construct. Build. Mater. 106 (Mar.1) (2016) 533–542.

[20] J.L. Zhou, C.X. Li, Z. Feng, et al., Experimental investigation on torsional behaviors of ultra-high-performance fiber-reinforced concrete hollow beams, Cem. Concr. Compos. 129 (2022), 104504.

[21] C. Zhou, J.Q. Wang, W.B. Jia, et al., Torsional behavior of ultra-high performance concrete (UHPC) rectangular beams without steel reinforcement: experimental investigation and theoretical analysis, Compos. Struct. 299 (2022), 116022.

[22] E. Fehling, M. Ismail, Experimental Investigations on UHPC Structural Elements Subject to Pure Torsion[C]//Ultra-high Performance Concrete and Nanotechnology in Construction, 2012.

[23] National Standard GB/T, 31387—2015 Reactive Powder Concrete, China Building Industry Press, Beijing, 2015.

[24] National Standard GB50010—2010 Code for Design of Concrete Structures, China Building Industry Press, Beijing, 2015.

[25] L.F.A. Bernardo, S.M.R. Lopes, Torsion in high-strength concrete hollow beams: strength and ductility analysis, ACI Struct. J. 106 (1) (2009) 39–48.

[26] M.M. Teixeira, L.F.A. Bernardo, Ductility of RC beams under torsion - ScienceDirect, Eng. Struct. 168 (2018) 759–769.

[27] A.M.T. Hassan, S.W. Jones, G.H. Mahmud, Experimental test methods to determine the uniaxial tensile and compressive behaviour of ultra-high performance fibre reinforced concrete (UHPFRC), Construct. Build. Mater. 37 (1) (2012) 874–882.

[28] T.T. Le, Ultra-high Performance Fibre Reinforced Concrete Paving flags[PhD], University of Liverpool, 2008.

[29] S.L. Gao, Study on Pseudo Strain-Hardening and Fracture Characteristic of Polyvinyl Alcohol Fiber Reinforced Cementitious Composites [PhD], Dalian University of Technology, 2006.

[30] Z.H. Yang, Study on Tensile Mechanical Properties of Reactive Steel Reinforced Concrete with Different Steel Fibers [PhD], Beijing Jiao tong University, 2006.

[31] D. Krajcinovic, J. Lemaitre, Continuum damage mechanics, theory and application, Int. Cent. Mech. Sci 295 (1) (1983) 68–74.

[32] Y.L. Chen, M. Zhong, Z.P. Chen, Pure torsional experiment and damage analysis of welded stud steel reinforced concrete beams, J. Build. Struct. 49 (2019) 110–117, 04.

[33] ACI 318-19, Building Code Requirements for Structural Concrete and Commentary, Farmington Hills, American Concrete Institute Committee, 2019.

[34] I. Kwahk, C. Joh, J.W. Lee, Torsional behavior design of UHPC box beams based on thin-walled tube theory, Engineering (3) (2015) 101–114, 07.

[35] T.T.C. Hsu, Torsion of Structural Concrete, Publication SP-18, ACI, 1968, pp. 261–306.